On the parametric X-rays along an emitting particle velocity

N. Nasonov *, A. Noskov

Laboratory of Radiation Physiks, Belgorod State University, 12 Studencheskaya Str., 308007 Belgorod, Russia

Abstract

Parametric X-rays along an emitting particle velocity is studied for the Bragg scattering geometry. The absence of discussed radiation yield in the case of thick enough target when an influence of a photoabsorption plays an important role is predicted. The correct boundary conditions for an emission field at the *out*-surface of absorbing semi-infinite crystalline target are discussed.

Keywords: Parametric X-rays; Dynamical diffraction theory; Spectral–angular distribution

1. Introduction

Theory of parametric X-rays (PXR) from relativistic particle in a crystal predicts an emission peak not only to the direction of Bragg scattering but along an emitting particle velocity as well [1–3]. Such additional peak (forward PXR) is of the great interest because of the discussed up to now question concerning its nature as Cherenkov like or scattering process [4]. In view of intensive attempts of the forward PXR experimental verification [5–7] the detailed theoretical description of this emission mechanism becomes central at present time.

Forward PXR for Laue scattering geometry attracts attention in the last theoretical work [8] devoted to discussed problem. PXR for Bragg scattering geometry is considered in our work on the basis of dynamical diffraction theory. Highly surprising result consisting in the absence of the forward PXR yield from thick enough absorbing target follows from our calculation. In addition to discussion of this result, the problem of correct boundary conditions for the forward PXR emission field at the out-surface of absorbing semi-infinite crystal is discussed. The principal difference between such conditions and those usually used in the case of PXR from semi-infinite crystal for Laue scattering geometry is shown.

In Section 2 the general expressions for emissions amplitude and spectral–angular distribution of emitted quanta are derived. The obtained results are used in Section 3 for analysis of the forward PXR features in the case of thin nonabsorbing crystal. Emission process in the limiting case of semi-infinite crystalline target is considered in Section 4 by the use of general expression derived

* Corresponding author. Tel.: +7-22-341477; fax: +7-22-341692.

E-mail address: nnn@bsu.edu.ru (N. Nasonov).

in Section 2 and within the frame of asymptotic approach. The effect of forward PXR suppression is discussed in that section. Our conclusions and some final comments are presented in Section 5.

2. General expressions

Let us consider an emission from relativistic electrons crossing a crystalline target with the thickness L and reflecting crystallographic plane parallel to the target surface as it is shown in Fig. 1. Electromagnetic field $\mathbf{E}(\mathbf{r},t)$ excited by the fast electron inside the crystal is described by the wave equation for Fourier transform of this field $\mathbf{E}_{\omega\mathbf{k}} = (2\pi)^{-4}\int \mathrm{d}t\,\mathrm{d}^3r\,\mathbf{E}(\mathbf{r},t)\,\mathrm{e}^{\mathrm{i}\omega t-\mathrm{i}\mathbf{k}\mathbf{r}}$,

$$(k^2-\omega^2(1+\chi_0))\mathbf{E}_{\omega\mathbf{k}} - \mathbf{k}(\mathbf{k}\mathbf{E}_{\omega\mathbf{k}}) - \omega^2\sum_{\mathbf{g}}{}'\chi_{-\mathbf{g}}\mathbf{E}_{\omega\mathbf{k}+\mathbf{g}} = \frac{\mathrm{i}\omega e}{2\pi^2}\mathbf{v}\delta(\omega-\mathbf{k}\mathbf{v}), \tag{1}$$

where $\mathbf{v}$ is the velocity of the fast electron, $\chi_0(\omega)$ and $\chi_{\mathbf{g}}(\omega)$ are the coefficients in the Fourier series for the crystal dielectric permeability $\varepsilon(\omega,\mathbf{r}) = 1+\chi_0(\omega)+\sum_{\mathbf{g}}{}'\chi_{\mathbf{g}(\omega)}\mathrm{e}^{\mathrm{i}\mathbf{g}\mathbf{r}}$, $\mathbf{g}$ are the reciprocal lattice vectors. Within the frame of used two wave approximation of dynamical diffraction theory [9] the Eq. (1) can be reduced to well known simple equations

$$(k^2-\omega^2(1+\chi_0))E_{\lambda 0} - \omega^2\chi_{-\mathbf{g}}\alpha_\lambda E_{\lambda\mathbf{g}} = \frac{\mathrm{i}\omega e}{2\pi^2}\mathbf{e}_{\lambda 0}\mathbf{v}\delta(\omega-\mathbf{k}\mathbf{v}), \tag{2}$$

$$((\mathbf{k}+\mathbf{g})^2-\omega^2(1+\chi_0))E_{\lambda\mathbf{g}} - \omega^2\chi_{\mathbf{g}}\alpha_\lambda E_{\lambda 0} = 0,$$

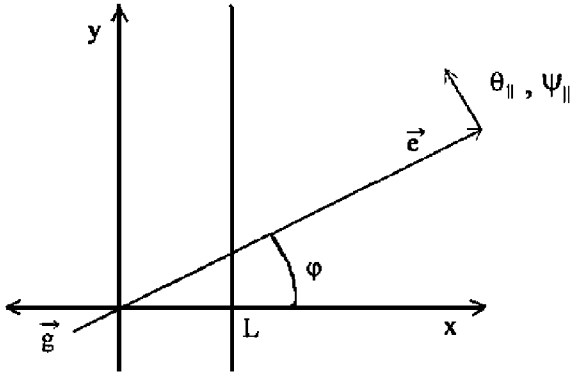

Fig. 1. Scattering geometry for the forward PXR.

where $\mathbf{E}_{\omega\mathbf{k}} = \sum_{\lambda=1}^{2}\mathbf{e}_{\lambda 0}E_{\lambda 0}$, $\mathbf{E}_{\omega\mathbf{k}+\mathbf{g}} = \sum_{\lambda=1}^{2}\mathbf{e}_{\lambda\mathbf{g}}E_{\lambda\mathbf{g}}$, $\mathbf{e}_{\lambda 0}$ and $\mathbf{e}_{\lambda\mathbf{g}}$ are the polarization vectors, $\mathbf{e}_{10}\sim[\mathbf{k},\mathbf{g}]$, $\mathbf{e}_{20}\sim[\mathbf{k},\mathbf{e}_{10}]$, $\mathbf{e}_{1\mathbf{g}}=\mathbf{e}_{10}$, $\mathbf{e}_{2\mathbf{g}}\sim[\mathbf{k}+\mathbf{g},\mathbf{e}_{10}]$, $\alpha_1=1$, $\alpha_2=\cos\varphi$. Equations for field components in a vacuum outside the crystal follow from (2) in the limit $\chi_0=\chi_{\mathbf{g}}=\chi_{-\mathbf{g}}=0$.

Since $\chi_0,\ \chi_{\mathbf{g}} \ll 1$, the dispersion equation for X-rays in a crystal slightly differs from that in a vacuum $k^2=\omega^2$, therefore it is convenient for further analysis to define the variable ξ by the expression

$$k_x = p+\xi, \quad \xi \ll p = \sqrt{\omega^2-k_\parallel^2},$$
$$\mathbf{k}_\parallel = \mathbf{e}_y k_y + \mathbf{e}_z k_z. \tag{3}$$

Using Eq. (3) and simplest approximation for susceptibilities,

$$\chi_0 = -\frac{\omega_0^2}{\omega^2}+\mathrm{i}\chi_0'', \quad \chi_{\mathbf{g}} = \chi_{-\mathbf{g}} = -\frac{\omega_{\mathbf{g}}^2}{\omega^2}+\mathrm{i}\chi_{\mathbf{g}}'', \tag{4}$$

where ω_0 is the plasma frequency of the crystal, $\omega_{\mathbf{g}}^2 = \omega_0^2(F(\mathbf{g})/Z)(S(\mathbf{g})/N_0)\mathrm{e}^{-(1/2)g^2u^2}$, $F(\mathbf{g})$ is the atom form-factor, Z is the number of electrons in an atom, $S(\mathbf{g})$ is the structure factor of an elementary cell containing N_0 atoms, u is the mean square amplitude of atom thermal vibrations, one can obtain the following general solutions of the Eq. (2) inside the crystal:

$$E_{\lambda 0}^{C} = b_{\lambda\mathbf{k}_\parallel}\delta(\xi-\xi_1) + c_{\lambda\mathbf{k}_\parallel}\delta(\xi-\xi_2) + \frac{\mathrm{i}\omega e}{4\pi^2 p v_x}\mathbf{e}_{\lambda 0}\mathbf{v}\frac{\xi-\frac{g^2}{2p}\left(1-2\frac{p}{g}-\frac{\omega^2}{g^2}\chi_0\right)}{(\xi-\xi_1)(\xi-\xi_2)}\delta(\xi-\xi_*),$$

$$E_{\lambda\mathbf{g}}^{C} = -\frac{\frac{\omega^2}{2p}\chi_{\mathbf{g}}\alpha_\lambda}{\xi-\frac{g^2}{2p}\left(1-2\frac{p}{g}-\frac{\omega^2}{g^2}\chi_0\right)}E_{\lambda 0} \tag{5}$$

in a vacuum in front of the crystal

$$E_{\lambda 0}^{i} = \frac{\mathrm{i}\omega e}{4\pi^2 p v_x}\mathbf{e}_{\lambda 0}\mathbf{v}\frac{1}{\xi}\delta(\xi-\xi_*), \tag{6}$$

and in a vacuum behind the crystal

$$E_{\lambda 0}^{f} = \frac{\mathrm{i}\omega e}{4\pi^2 p v_x}\mathbf{e}_{\lambda 0}\mathbf{v}\frac{1}{\xi}\delta(\xi-\xi_*) + a_{\lambda\mathbf{k}_\parallel}\delta(\xi). \tag{7}$$

The very important quantities $\xi_{1,2}$ and ξ_* are defined as

$$\xi_{1,2} = -\frac{\omega_0^2}{2p} + \frac{\omega_{\mathbf{g}}^2}{2p}\alpha_\lambda\left[\tau_\lambda \pm \sqrt{\tau_\lambda^2 - 1 - 2\mathrm{i}\delta_\lambda(\tau_\lambda - \kappa_\lambda)}\right],$$

$$\tau_\lambda = \frac{g^2}{2\omega_{\mathbf{g}}^2\alpha_\lambda}\left(1 - 2\frac{p}{g} + 2\frac{\omega_0^2}{g^2}\right),$$

$$\delta_\lambda = \frac{\omega^2\chi_0''}{\omega_{\mathbf{g}}^2\alpha_\lambda}, \quad \kappa_\lambda = \frac{\chi_{\mathbf{g}}''}{\chi_0''}\alpha_\lambda,$$

$$\xi_* = \frac{1}{v_x}(\omega - \mathbf{k}_\parallel\mathbf{v}_\parallel - pv_x). \tag{8}$$

Unknown coefficients $a_{\lambda\mathbf{k}_\parallel}$, $b_{\lambda\mathbf{k}_\parallel}$ and $c_{\lambda\mathbf{k}_\parallel}$ are determined by the ordinary boundary conditions

$$\int \mathrm{d}\xi(E_{\lambda 0}^C - E_{\lambda 0}^i) = \int \mathrm{d}\xi\,\mathrm{e}^{\mathrm{i}\xi L}E_{\lambda\mathbf{g}}^C = \int \mathrm{d}\xi\,\mathrm{e}^{\mathrm{i}\xi L}(E_{\lambda 0}^C - E_{\lambda 0}^f) = 0. \tag{9}$$

The final expression for the coefficient $a_{\lambda\mathbf{k}_\parallel}$ determining an emission field takes the form

$$\begin{aligned} a_{\lambda\mathbf{k}_\parallel} = {} & \frac{\mathrm{i}\omega e}{4\pi^2 pv_x}\frac{\mathbf{e}_{\lambda 0}\mathbf{v}}{D}\mathrm{e}^{\mathrm{i}\xi_* L}\left[\left(\frac{1}{\xi_*} - \frac{1}{\xi_* - \xi_2}\right)\right. \\ & \times\left(1 - \mathrm{e}^{-\mathrm{i}(\xi_* - \xi_2)L}\right)\left(\xi_2 - \frac{g^2}{2p}\left(1 - 2\frac{p}{g} - \frac{\omega^2}{g^2}\chi_0\right)\right) \\ & \times\mathrm{e}^{-\mathrm{i}(\xi_* - \xi_1)L} - \left(\frac{1}{\xi_*} - \frac{1}{\xi_* - \xi_1}\right)\left(1 - \mathrm{e}^{-\mathrm{i}(\xi_* - \xi_1)L}\right) \\ & \left.\times\left(\xi_1 - \frac{g^2}{2p}\left(1 - 2\frac{p}{g} - \frac{\omega^2}{g^2}\chi_0\right)\right)\mathrm{e}^{-\mathrm{i}(\xi_* - \xi_2)L}\right], \end{aligned}$$

$$\begin{aligned} D = {} & \left(\xi_1 - \frac{g^2}{2p}\left(1 - 2\frac{p}{g} - \frac{\omega^2}{g^2}\chi_0\right)\right)\mathrm{e}^{-\mathrm{i}(\xi_* - \xi_2)L} \\ & - \left(\xi_2 - \frac{g^2}{2p}\left(1 - 2\frac{p}{g} - \frac{\omega^2}{g^2}\chi_0\right)\right)\mathrm{e}^{-\mathrm{i}(\xi_* - \xi_1)L}. \end{aligned} \tag{10}$$

Using the obtained result (10) one can determine the emission amplitude A_λ by the calculation of Fourier integral in the wave zone,

$$E_\omega^{\mathrm{Rad}} = \int \mathrm{d}^3k\,\mathrm{e}^{\mathrm{i}\mathbf{k}\mathbf{n}r}a_{\lambda\mathbf{k}_\parallel}\delta(\xi) \to A_\lambda\frac{\mathrm{e}^{\mathrm{i}\omega r}}{r},$$

$$A_\lambda = -2\pi\mathrm{i}\omega n_x a_{\lambda\omega\mathbf{n}_\parallel}, \tag{11}$$

where $\mathbf{n}$ is the unit vector along the direction of emitted photon propagation, $\mathbf{n} = \mathbf{e}_x n_x + \mathbf{n}_\parallel$, $\mathbf{e}_x\mathbf{n}_\parallel = 0$, integral (11) has been taken by the use of stationary phase method.

Formulae (8), (10) and (11) allow to describe all spectral and angular characteristics of the forward PXR. Before proceeding to the analysis of such characteristics one should take into account that three emission mechanisms make the contribution to the formation of total emission yield: bremsstrahlung, transition radiation (TR) and forward PXR. The amplitude A_λ includes the contribution of forward PXR and TR. Since the TR being background is the main obstacle for the forward PXR experimental verification it is very important to represent the amplitude A_λ as a sum of PXR and TR amplitudes. Such representation allows to estimate the relative contributions from the discussed emission mechanisms as well as an interference between them. Defining the angular variables $\boldsymbol{\Theta}$ and $\boldsymbol{\Psi}$ in accordance with formulae (see Fig. 1)

$$\mathbf{n} = \mathbf{e}\left(1 - \frac{1}{2}\Theta^2\right) + \boldsymbol{\Theta}, \quad \mathbf{e}\boldsymbol{\Theta} = \mathbf{0},$$

$$\mathbf{v} = \mathbf{e}\left(1 - \frac{1}{2}\gamma^{-2} - \frac{1}{2}\Psi^2\right) + \boldsymbol{\Psi}, \quad \mathbf{e}\boldsymbol{\Psi} = 0, \tag{12}$$

one can obtain the following expression for the emission spectral–angular distribution:

$$\omega\frac{\mathrm{d}N_\lambda}{\mathrm{d}\omega\,\mathrm{d}^2\theta} = \left\langle\left|A_\lambda^{\mathrm{PXR}} + A_\lambda^{\mathrm{TR}}\right|^2\right\rangle,$$

$$\begin{aligned} A_\lambda^{\mathrm{PXR}} = {} & \frac{e}{\pi}\frac{\frac{\omega_{\mathbf{g}}^2}{\omega^2}\alpha_\lambda\Omega_\lambda}{\gamma^{-2} + \frac{\omega_0^2}{\omega^2} + \Omega^2}\left\{\frac{1}{\sigma_-}\left[1 - \mathrm{e}^{-\frac{\mathrm{i}\omega L}{2\sin\varphi}\sigma_-}\right]\mathrm{e}^{\frac{\mathrm{i}\omega_{\mathbf{g}}^2 L\alpha_\lambda}{2\omega\sin\varphi}f_\lambda}\right. \\ & \left.- \frac{1}{\sigma_+}\left[1 - \mathrm{e}^{-\frac{\mathrm{i}\omega L}{2\sin\varphi}\sigma_+}\right]\mathrm{e}^{-\frac{\mathrm{i}\omega_{\mathbf{g}}^2 L\alpha_\lambda}{2\omega\sin\varphi}f_\lambda}\right\}\frac{1}{D}, \end{aligned}$$

$$\begin{aligned} A_\lambda^{\mathrm{TR}} = {} & \frac{e}{\pi}\Omega_\lambda\left(\frac{1}{\gamma^{-2} + \Omega^2} - \frac{1}{\gamma^{-2} + \frac{\omega_0^2}{\omega^2} + \Omega^2}\right) \\ & \times\left\{1 + 2\frac{f_\lambda}{D}\mathrm{e}^{-\frac{\mathrm{i}\omega L}{2\sin\varphi}\left(\gamma^{-2} + \frac{\omega_0^2}{\omega^2} + \Omega^2 - \frac{\omega_{\mathbf{g}}^2}{\omega^2}\alpha_\lambda\tau_\lambda\right)}\right\}, \end{aligned}$$

$$\begin{aligned} D = {} & (\tau_\lambda - f_\lambda - \mathrm{i}\delta_\lambda)\mathrm{e}^{-\frac{\mathrm{i}\omega_{\mathbf{g}}^2 L\alpha_\lambda}{2\omega\sin\varphi}f_\lambda} \\ & - (\tau_\lambda + f_\lambda - \mathrm{i}\delta_\lambda)\mathrm{e}^{\frac{\mathrm{i}\omega_{\mathbf{g}}^2 L\alpha_\lambda}{2\omega\sin\varphi}f_\lambda}, \end{aligned} \tag{13}$$

where the quantity f_λ coincides with square root in the definitions (8), $\sigma_\pm = \gamma^{-2} + (\omega_0^2/\omega^2) + \Omega^2 - (\omega_g^2/\omega^2)\alpha_\lambda(\tau_\lambda \pm f_\lambda)$, $\Omega_1 = \Theta_\perp - \Psi_\perp$, $\Omega_2 = \Theta_\parallel - \Psi_\parallel$, $\Omega^2 = \Omega_1^2 + \Omega_2^2$, brackets $\langle\rangle$ mean averaging over angles $\Psi_\perp$ and $\Psi_\parallel$ describing the angular spread of an electron beam.

The obtained result (13) provides a basis for the further analysis.

3. Forward PXR from a thin nonabsorbing target

First of all let us consider the emission properties in the relatively simple case of thin enough target ($(\omega L/2\sin\varphi)\chi_0''(\omega) \ll 1$), when the absorption coefficient δ_λ in (13) can be neglected. In accordance with the expression for A_λ^{PXR} (see Eq. (13)) two branches of possible X-ray waves in a crystal make the contribution to the forward PXR yield, but on the condition $\delta_\lambda = 0$ under consideration only the contribution from one of them corresponding to the denominator σ_+ can be essential because the equation $\sigma_+(\omega, \boldsymbol{\Theta}) = \mathbf{0}$ has a solution in contrast with the equation $\sigma_-(\omega, \boldsymbol{\Theta}) = \mathbf{0}$, which has no solutions (the situation can change dramatically in the case of a thick absorbing crystal as it will be shown later). Spectral–angular distribution of the separate PXR yield follows from (13) in the form

$$\omega\frac{\mathrm{d}N_\lambda^{\mathrm{PXR}}}{\mathrm{d}\omega\,\mathrm{d}^2\theta} = \frac{e^2}{\pi^2}\left\langle \frac{\Omega_\lambda^2}{\left(\gamma^{-2} + \frac{\omega_0^2}{\omega^2} + \Omega^2\right)^2} R_\lambda^{\mathrm{PXR}} \right\rangle,$$

$$R_\lambda^{\mathrm{PXR}} = \frac{1}{\tau_\lambda^2 - 1 + \sin^2\left(\frac{\omega_g^2 L\alpha_\lambda}{2\omega\sin\varphi}\sqrt{\tau_\lambda^2 - 1}\right)} \times \frac{\sin^2\left(\frac{\omega_g^2 L\alpha_\lambda}{4\omega\sin\varphi}\left(\beta_\lambda - \tau_\lambda - \sqrt{\tau_\lambda^2 - 1}\right)\right)}{\left(\beta_\lambda - \tau_\lambda - \sqrt{\tau_\lambda^2 - 1}\right)^2}, \tag{14}$$

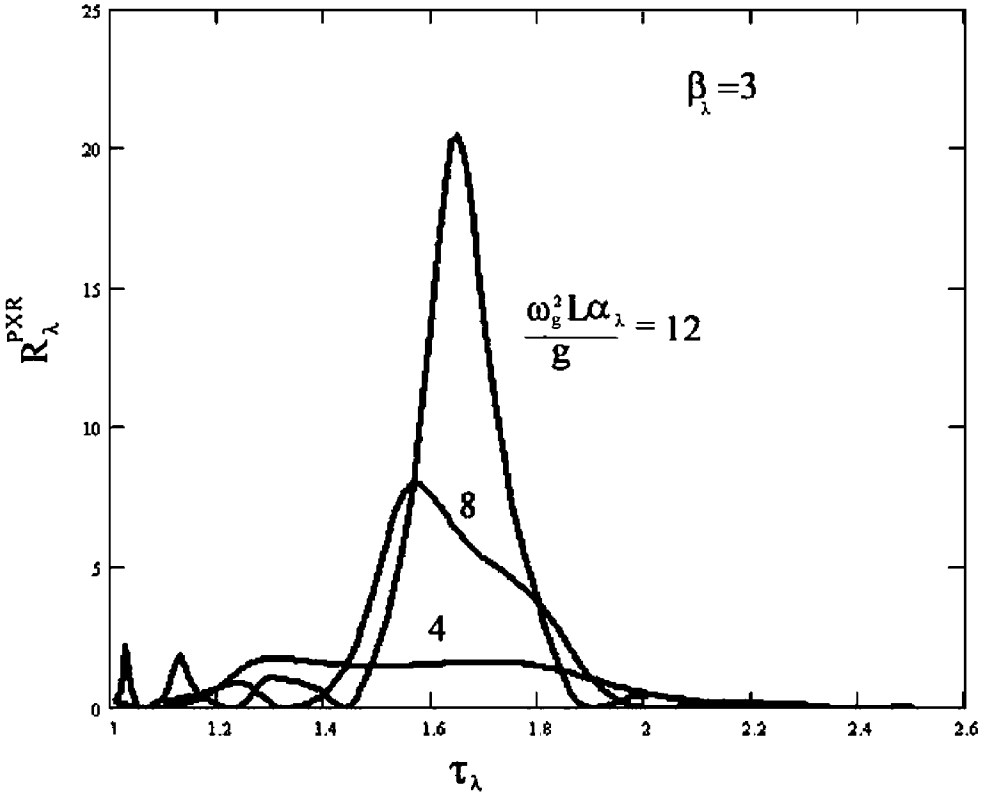

Fig. 2. PXR "natural" spectrum versus the thickness of the target.

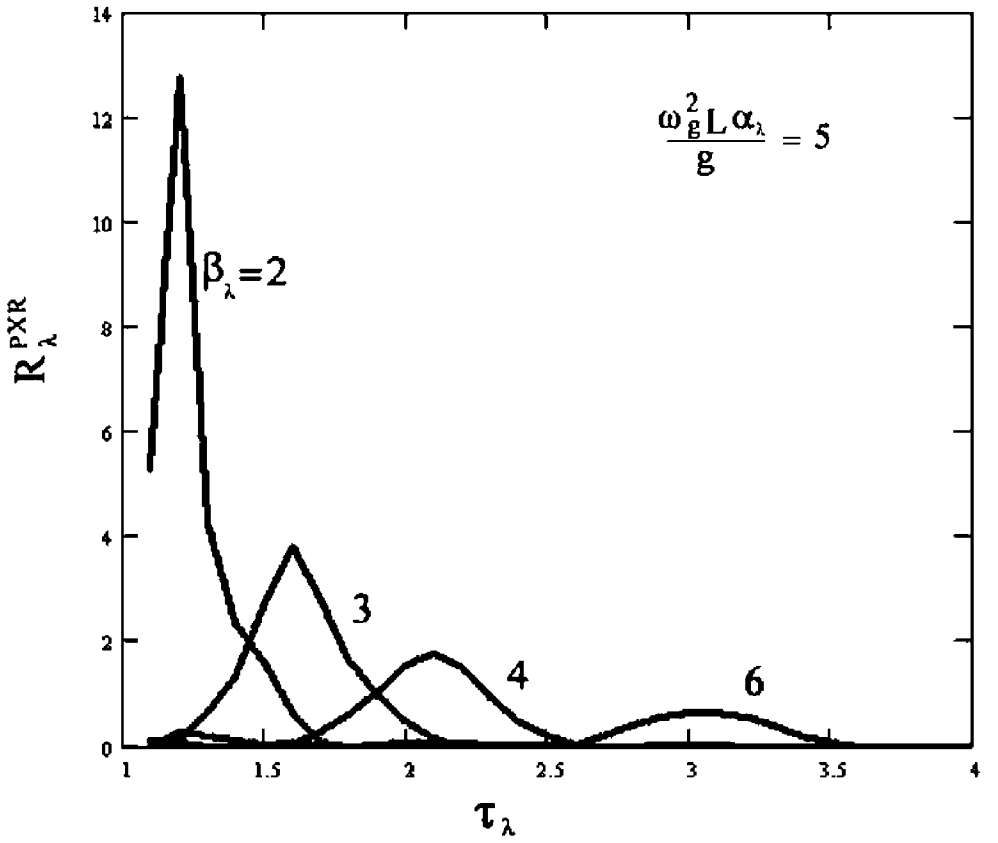

Fig. 3. PXR "natural" spectrum versus the observation angle and the energy of emitting particle.

where $\beta_\lambda = (\omega^2/\omega_g^2\alpha_\lambda)(\gamma^{-2} + \frac{\omega_0^2}{\omega^2} + \Omega^2) > 1$, this expression is correct in the range $\tau_\lambda^2 > 1$. [1]

Considering the quantity $\tau_\lambda(\omega, \Theta)$ defined in (8) one can see that this quantity can be represented as

$$\tau_\lambda \approx \frac{g^2}{2\omega_g^2\alpha_\lambda}\left(1 - \frac{\omega}{\omega'_B}\right), \quad \omega'_B = \frac{\omega_B}{1 + \theta_\parallel \cot\varphi}, \quad (15)$$

where $\omega_B = g/2\sin\varphi$ is the Bragg frequency. Since $\omega_g^2/g^2 \ll 1$ the dependence $\tau_\lambda(\omega)$ is the "fast function" of ω, therefore it is very convenient to consider $\tau_\lambda(\omega)$ as new spectral variable instead of ω for an analysis of PXR spectral properties. As this takes a place $\omega(\tau_\lambda) = \omega'_B(1 - 2(\omega_g^2/g^2)\alpha_\lambda\tau_\lambda) \approx \omega'_B \approx \omega_B$ in the vicinity of Bragg frequency where PXR can be realized. Thus, the function R_λ^{PXR} in (14) describes PXR "natural spectrum" which can be observed at fixed observation angle Θ. This spectrum is illustrated by the curves in Figs. 2 and 3 calculated for different values of the parameters β_λ and $\omega_g^2 L\alpha_\lambda/g$. The curves presented in Fig. 2 demonstrate the growth of the amplitude of PXR peak and decreasing of its spectral width when the crystal thickness L increases. More interesting behaviour of PXR spectrum is illustrated by the curves in Fig. 3. The maximum of this spectral peak is shifted to the side of the anomalous dispersion range $|\tau_\lambda| < 1$ with decreasing of the parameter β_λ (the role of dynamical diffraction increases when β_λ decreases). On the other hand this maximum is always placed inside the range of anomalous dispersion as it follows from the equation $\sigma_+ = 0$,

$$\tau_\lambda = \tau_{\lambda *} = 1 + \frac{(\beta_\lambda - 1)^2}{2\beta_\lambda} > 1, \quad (16)$$

[1] It is necessary to point to the fact that $R_\lambda^{PXR} \to \infty$ if $\tau_\lambda \to 1$, but this singularity has no physical sense because the total PXR amplitude A_λ^{PXR} in (13) is regular in this point.

therefore the expression (14) derived under condition $\tau_\lambda > 1$ is sufficient for the forward PXR description.

The formula for PXR angular distribution follows from Eq. (14) after integration over photon energies ω (since PXR spectral peak is very narrow on condition $\omega_g^2 L/g \gg 1$ under consideration one can use the well known approximation $\sin^2(TX)/x^2 \to \pi T\delta(x)$) in the form

$$\frac{1}{L}\frac{dN_\lambda^{PXR}}{d^2\theta} = \frac{2e^2\omega_g^8\alpha_\lambda^4}{\pi g^3\omega_B^4} \times \left\langle \frac{\Omega_\lambda^2}{\left(\gamma^{-2}+\frac{\omega_0^2}{\omega_B^2}+\Omega^2\right)^2\left[\left(\gamma^{-2}+\frac{\omega_0^2}{\omega_B^2}+\Omega^2\right)^2-\frac{\omega_g^4}{\omega_B^4}\alpha_\lambda^2\right]} \times \frac{1}{1+\left(\frac{2\beta_\lambda}{\beta_\lambda^2-1}\right)^2\sin^2\left(\frac{\omega_g^2 L\alpha_\lambda}{g}\,\frac{\beta_\lambda^2-1}{2\beta_\lambda}\right)} \right\rangle. \quad (17)$$

The expression (17) shows that the forward PXR angular density can be essential on condition $\gamma > \gamma_* = \omega_B/\omega_0$ only when the dynamical diffraction effects occur in PXR process [8]. Within the range of small emitting particle energies $\gamma \ll \gamma_*$ the estimation $(dN_\lambda^{PXR}/d^2\theta) \sim \gamma^6/\gamma_*^6 \ll 1$ follows for the distribution (17) in the vicinity of its maximum. The forward PXR angular distribution calculated in (17) in the most interesting case of high energy particle $\gamma \gg \gamma_*$ when this distribution does not depend on γ is illustrated by the curves presented in Fig. 4. Two parameters $\omega_g^2 L\alpha_\lambda/g$ and $\omega_g^2\alpha_\lambda/\omega_0^2$ determine such distribution, which is shifted to small observation angles relative to angular distribution of ordinary PXR propagating to Bragg scattering direction (indeed the maximum of the ordinary PXR angular distribution corresponds to the observation angle $\theta = \theta_* = \omega_0/\omega_B = \gamma_*^{-1}$ if $\gamma \gg \gamma_*$). More surprising behaviour of the distribution (17) consists in the strong oscillations of PXR angular density as it follows from Fig. 4. These oscillations appear due to an interference between two branches of excited X-ray waves forming together with a fast particle equilibrium electromagnetic field the total emission field behind the crystal (connection between these branches is described by the denominator D in the general expression (13)).

Since in the real experiment PXR contribution can be observed on the background of TR only, it is necessary to analyse the separate TR contribution and the influence of an interference between

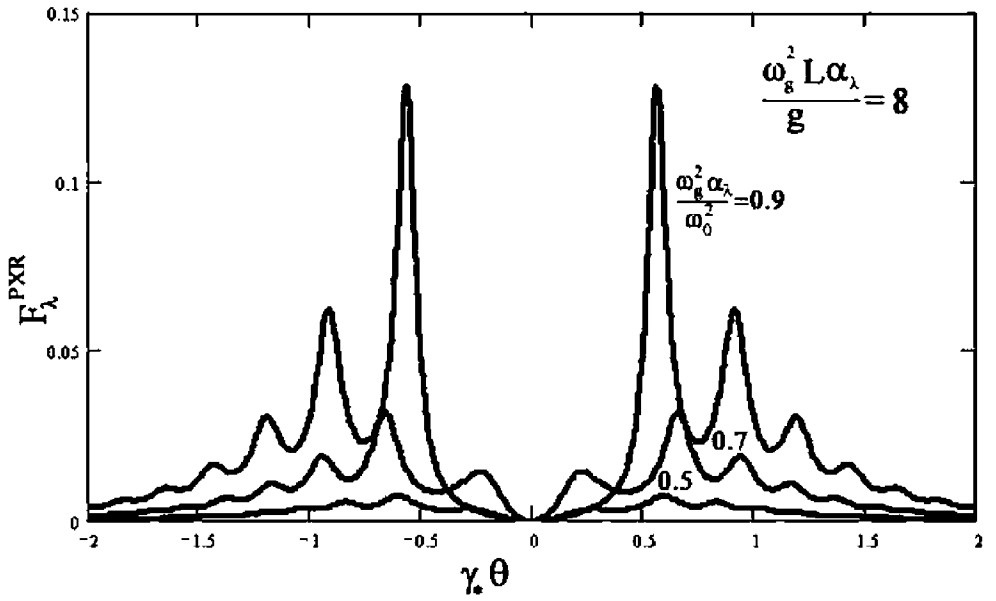

Fig. 4. PXR angular distribution. The function F_λ^{PXR} is proportional to $dN_\lambda^{PXR}/d^2\theta$.

PXR and TR. It should be noted that the effect of PXR and TR interference has been discussed in detail in [10,11], but for PXR in Bragg scattering direction only. Obviously such an interference manifestation is the same in the case under consideration. Coming back to the general formula (13) one can obtain the following expression for TR spectral–angular distribution:

$$\omega\frac{\mathrm{d}N_\lambda^{\mathrm{TR}}}{\mathrm{d}\omega\,\mathrm{d}^2\theta} = \frac{e^2}{\pi^2}\left\langle \Omega_\lambda^2\left(\frac{1}{\gamma^{-2}+\Omega^2}-\frac{1}{\gamma^{-2}+\frac{\omega_0^2}{\omega^2}+\Omega^2}\right)^2 R_\lambda^{\mathrm{TR}}\right\rangle,$$

$$R_\lambda^{\mathrm{TR}} = 1+\frac{\tau_\lambda^2-1}{\tau_\lambda^2-1+\sin^2\left(\frac{\omega_{\mathrm{g}}^2 L\alpha_\lambda}{2\omega\sin\varphi}\sqrt{\tau_\lambda^2-1}\right)} \times\left[1-2\left(\cos\left(\frac{\omega_{\mathrm{g}}^2 L\alpha_\lambda}{2\omega\sin\varphi}\sqrt{\tau_\lambda^2-1}\right)\times\cos\left(\frac{\omega_{\mathrm{g}}^2 L\alpha_\lambda}{2\omega\sin\varphi}(\beta_\lambda-\tau_\lambda)\right)-\frac{\tau_\lambda}{\sqrt{\tau_\lambda^2-1}}\sin\left(\frac{\omega_{\mathrm{g}}^2 L\alpha_\lambda}{2\omega\sin\varphi}\sqrt{\tau_\lambda^2-1}\right)\times\sin\left(\frac{\omega_{\mathrm{g}}^2 L\alpha_\lambda}{2\omega\sin\varphi}(\beta_\lambda-\tau_\lambda)\right)\right)\right]. \quad (18)$$

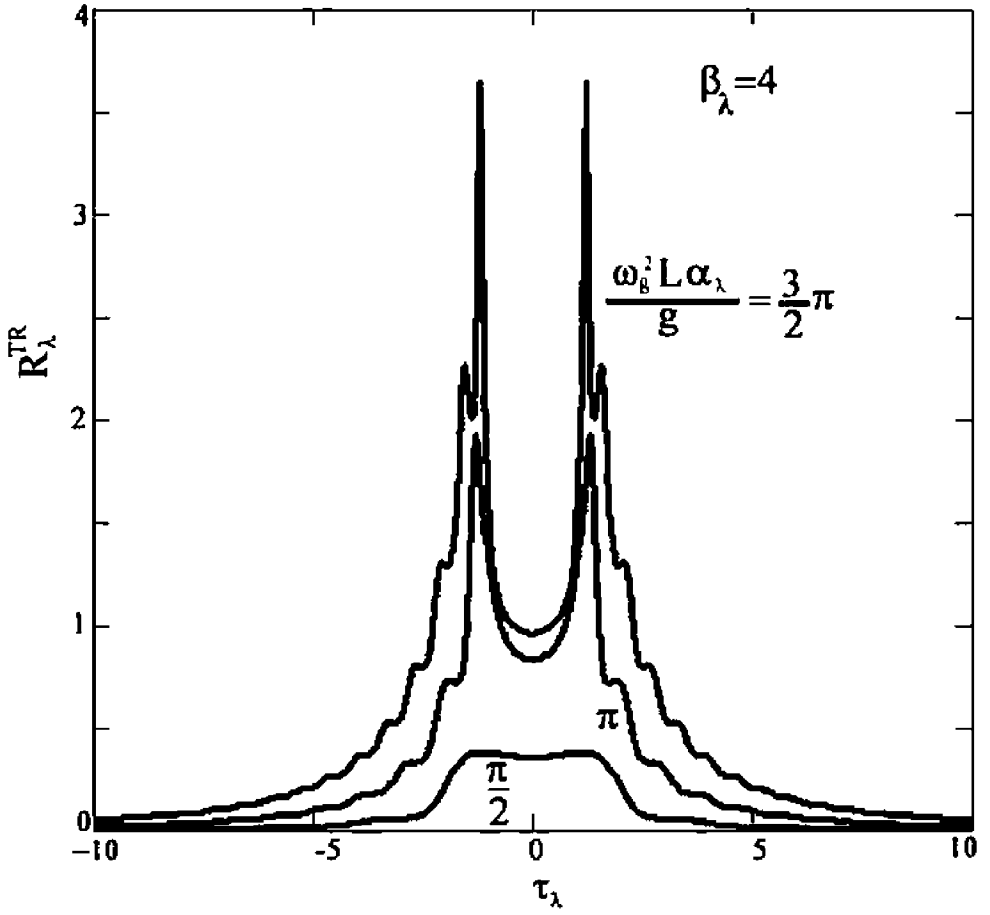

Fig. 5. DTR "natural" spectrum versus the thickness of the target.

Distribution (18) (it should be noted that this formula is valid for all possible values of the quantity τ_λ) differs essentially from that of an ordinary TR emitted from an amorphous dielectric plate with the thickness L, but such differences caused by the dynamical diffraction effects take place in the vicinity of Bragg frequency ω_B only, where the "fast variable" $\tau_\lambda(\omega)$ takes the values $|\tau_\lambda| \leqslant 1$. Inside the vicinity of Bragg frequency ($|\tau_\lambda| \gg 1$) the function R_λ^{TR} is reduced to well known expression

$$R_\lambda^{TR} \to 2\left[1 - \cos\left(\frac{\omega_g^2 L\alpha_\lambda}{2\omega\sin\varphi}\beta_\lambda\right)\right] \equiv 2\left[1 - \cos\left(\frac{\omega L}{2\sin\varphi}\left(\gamma^{-2} + \frac{\omega_0^2}{\omega^2} + \Omega^2\right)\right)\right], \tag{19}$$

describing the interference between TR waves emitted from in and out-surfaces of the target.

In accordance with formulae (18) and (19) TR spectrum is very wide in contrast with PXR spectrum (14), therefore X-ray detector with high energy resolution must be used in the experiment devoted to forward PXR observation. The result (19) shows an interesting possibility to reduce TR contribution to total emission yield in the vicinity of Bragg frequency where the forward PXR is realized. Indeed, the contribution of ordinary TR is suppressed in the wide vicinity of Bragg frequency ω_B for fixed observation angle in view of

$$\frac{\omega_g^2 L\alpha_\lambda}{2\omega_B\sin\varphi}\beta_\lambda \equiv \frac{gL}{4\sin^2\varphi}\left(\gamma^{-2} + \frac{\omega_0^2}{\omega_B^2} + \Omega^2\right) = 2\pi n. \tag{20}$$

The function $R_\lambda^{TR}(\tau_\lambda)$ calculated by (18) for fixed value of the parameter β_λ and different values of the parameter $\omega_g^2 L\alpha_\lambda/g$ is presented in Fig. 5. The calculated narrow TR peak is analogous to that predicted in [12]. In the range of anomalous dispersion $|\tau_\lambda(\omega)| < 1$ it consists of TR wave emitted from the out-surface of the target only because of the total reflection within the range $|\tau_\lambda| < 1$ of TR wave emitted from *in*-surface of the target.

On condition (20) under consideration TR and PXR are realized as single spectral peaks located close to each other. Their angular distributions are rather different in the range of high enough emitting particle energies $\gamma \gg \gamma_*$. In accordance with Eq. (18) maximum of TR angular distribution is located near the angle $\Theta \approx \gamma^{-1}$. On the other hand PXR angular distribution is concentrated in the range of larger angles $\Theta \sim \gamma_*^{-1} \gg \gamma^{-1}$ as it follows from Fig. 4. Thus the relation between contributions of collimated TR and forward PXR depends strongly on the observation angle $\boldsymbol{\Theta}$. To consider such a relation it is necessary to take into account an interference between PXR and TR as well. Coming back to the general formula (13) one can obtain the following expression for interference term:

$$\omega\frac{dN_\lambda^{INT}}{d\omega\, d^2\theta} = \frac{2e^2\omega_g^2\alpha_\lambda}{\pi^2\omega^2}\left\langle \frac{\Omega_\lambda^2}{\left(\gamma^{-2} + \frac{\omega_0^2}{\omega^2} + \Omega^2\right)^2} \times \frac{1}{\tau_\lambda^2 - 1 + \sin^2\left(\frac{\omega_g^2 L\alpha_\lambda}{2\omega\sin\varphi}\sqrt{\tau_\lambda^2 - 1}\right)} \times \left[\frac{\omega_0^2}{\omega^2}\left(\tau_\lambda + \sqrt{\tau_\lambda^2 - 1}\right) \times \sin\left(\frac{\omega_g^2 L\alpha_\lambda}{2\omega\sin\varphi}\sqrt{\tau_\lambda^2 - 1}\right) \times \frac{\cos\left(\frac{\omega L}{4\sin\varphi}\sigma_-\right)}{\gamma^{-2} + \Omega^2} - \frac{\omega_g^2}{\omega^2}\alpha_\lambda\cos\left(\frac{\omega_g^2 L\alpha_\lambda}{2\omega\sin\varphi}\sqrt{\tau_\lambda^2 - 1}\right) \times \frac{\sin\left(\frac{\omega L}{4\sin\varphi}\sigma_-\right)}{\sigma_-}\right] \frac{\sin\left(\frac{\omega L}{4\sin\varphi}\sigma_+\right)}{\sigma_+}\right\rangle. \tag{21}$$

Formula (21) contains the main terms only which is to say that the crystal thickness L exceeds the extinction length ω/ω_g^2. The first term in square brackets in (21) describes an interference between PXR and TR, the second one corresponds to an interference between two different branches of PXR waves. This formula is valid within the range $\tau_\lambda > 1$ where PXR contribution is essential.

Formulae (14), (18) and (21) allow to analyze the possibility to separate PXR contribution from the total emission yield on the basis of proposed approach consisting in the measurement of strongly collimated radiation by the use of X-ray detector with high energy resolution (a crystal-diffractometer can be convenient for this purpose). Spectral–angular distributions of TR, forward PXR and interference term calculated by (14), (18) and (21) with the assumptions that $\gamma \gg \gamma_*$ and the condition (20) is fulfilled are presented in Fig. 6. First of all the presented curves demonstrate a small influence of an interference between PXR and TR. Since the widths of TR and PXR peaks are very small (about several eV) the total number of photons emitted by TR and PXR mechanisms has to be registered at the real experiment. Therefore the narrow spectral peak which can be observed in the range of small observation angles $\Theta < \gamma_*^{-1}$ is formed mainly by TR contribution in accordance with Fig. 6. On the other hand relative PXR contribution increases with increasing of the observation angle Θ as it follows from Fig. 6, but the total emission yield decreases essentially in this case.

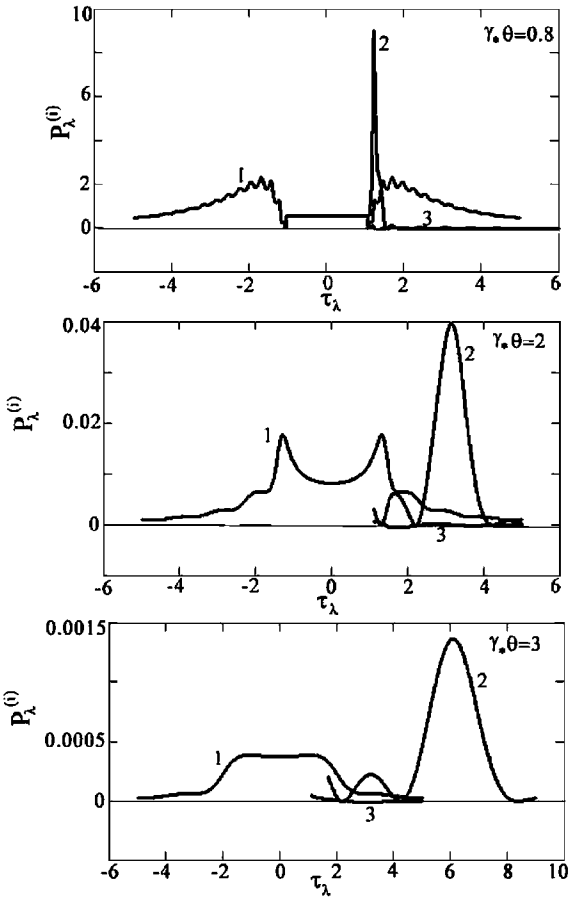

Fig. 6. Relative contributions of DTR, PXR, and the interference term to the total emission spectral–angular distribution. Presented functions $P_\lambda^{(i)}$ are determined by the formula $P_\lambda^{(i)} = (\pi^2/e^2)(\omega_0^2/\omega)(\mathrm{d}N_\lambda^{(i)}/\mathrm{d}\omega\,\mathrm{d}^2\theta)$. Curve 1 corresponding to the function P_λ^1 describes DTR spectral–angular distributions, curve 2 describes PXR, curve 3 corresponds to the interference term. All curves were calculated for fixed value of the parameter $\omega_g^2\alpha_\lambda/\omega_0^2 = 0.8$ The thickness of the target L and the observation angle θ are connected by resonance condition (20) for $n = 3$.

4. Forward PXR from the thick absorbing target

Since PXR contribution increases with increasing of the thickness of a target it is interesting to consider the limiting case of semi-infinite crystal used often for the analysis of general PXR properties [4,11]. Again coming back to the general result (13) and taking into account the definitions (8) one can reduce the expressions (13) for A_λ^{PXR} and A_λ^{TR} in the limit $Ł \to \infty$ to very simple formulae

$$A_\lambda^{\mathrm{PXR}} = -\frac{e}{\pi}\frac{\omega_g^2}{\omega^2}\alpha_\lambda \frac{\Omega_\lambda^2}{\gamma^{-2} + \frac{\omega_0^2}{\omega^2} + \Omega^2} \times \frac{1}{\sigma_-} \times \frac{1}{\tau_\lambda + f_\lambda - \mathrm{i}\delta_\lambda},$$

$$A_\lambda^{\mathrm{TR}} = \frac{e}{\pi}\Omega_\lambda \left(\frac{1}{\gamma^{-2} + \Omega^2} - \frac{1}{\gamma^{-2} + \frac{\omega_0^2}{\omega^2} + \Omega^2} \right). \qquad (22)$$

Amplitude A_λ^{TR} in (22) is the ordinary emission amplitude of TR from a relativistic particle, crossing a single boundary between vacuum and medium. On the other hand the amplitude A_λ^{PXR} differs essentially from that following from PXR theory for Laue geometry and semi-infinite target. Only one branch of solutions of the wave equation makes the contribution to PXR yield, which is negligibly small because the quantity $Re[\sigma_-]$ is always nonzero.

To explain this unexpected result let us discuss general formulae (5) describing the total electromagnetic field inside the crystalline target. In accordance with (5) the primary field $E^C_{\lambda 0}$ is formed by the particle Coulomb field transformed due to scattering on crystalline electrons and by two free X-ray waves corresponding to different branches of the solution of dispersion equation. In the case of Laue scattering geometry the unknown coefficient $b_{\lambda \mathbf{k}_\parallel}$ and $c_{\lambda \mathbf{k}_\parallel}$ in (5) are completely determined by well known boundary conditions for the primary $E^C_{\lambda 0}$ and diffracted field $E^C_{\lambda \mathbf{g}}$ at in-surface of a target. Since in the case of Laue geometry all free waves are damped out to the direction from in- to out-surface of the target [14], only the particle equilibrium field can be essential at the exit of a target in the limiting case of a thick crystal with the thickness L greater than an absorption length. As this takes place, the forward PXR field in vacuum behind the crystal $E^f_{\lambda 0}$ is determined in the case under consideration by the last boundary condition (9), where the field $E^C_{\lambda 0}$ contains the particle equilibrium field only [13].

Such approach allowing to obtain the very simple solution of the task of PXR description in the case of Laue geometry fails for Bragg geometry. First of all it should be noted that the field inside the crystal can not be completely determined in the case of Bragg geometry by the boundary conditions at in-surface of the target only. Furthermore, in the limiting case $L \to \infty$ one cannot use the particle equilibrium field as the total electromagnetic field inside the target in boundary conditions at out-surface of the target in contrast with PXR for Laue geometry. Indeed, the diffracted component of the particle equilibrium field does not satisfy to second boundary condition (9), therefore one must use an additional contribution of free X-ray waves in this boundary condition.

Let as consider in more detail the role of free waves in the formation of PXR yield in the case of Bragg geometry. In accordance with the expression (8) defining quantities $\xi_{1,2}$ within the frequency range $\tau_\lambda(\omega) > 1$, where the forward PXR can be realized the free wave corresponding to $k_x = k_{2x} = p + \xi_2 = \omega n_x + \xi_2$ is damped to the direction from in- to out-surface of a target. But another wave corresponding to $k_{1x} = \omega n_x + \xi_1$ is damped in a reverse direction from the first wave. Therefore this wave can not be excited at the in-surface of a target. Calculation of the group velocity performed by the use of the expression for $\xi(\omega)$ in (8) leads to the conclusion that this velocity $(\partial k_{1,2x}/\partial\omega)^{-1} \approx \mp\sqrt{\tau_\lambda^2 - 1}/n_x\tau_\lambda$ is negative for the discussed wave with anomalous direction of damping. Therefore the energy carried by this wave is transferred from out- to in-surface of the target. This circumstance leads to the suppression of PXR in the case of thick enough crystal when the transferred energy is totally absorbed.

Based on the presented consideration the solution of discussed task in the case of semi-infinite target can be found within the frame of very simple approach. Neglecting the free wave corresponding to ξ_2 in the general solution (5) and using only two last boundary conditions in (9) one can obtain the very simple expression for the coefficient $a_{\lambda \mathbf{k}_\parallel}$,

$$a_{\lambda \mathbf{k}_\parallel} = \frac{\mathrm{i}\omega e}{4\pi^2 p v_x} \mathbf{e}_{\lambda 0}\mathbf{v}\left(\frac{\mathbf{1}}{\xi_* - \xi_{\mathbf{2}}} - \frac{\mathbf{1}}{\xi_*}\right), \tag{23}$$

which coincides with that following from the general solution (10) in the limiting case $L \to \infty$. Obviously, expressions (22) and (23) are equivalent.

5. Conclusions

The above-described results demonstrate a possibility to observe the forward PXR from relativistic electrons crossing a crystalline target oriented so, that the Bragg scattering geometry can be realized. The most appropriate conditions for observation of such an effect are realized in the case of thin enough target with the thickness L less than an absorption length. In the opposite case of thick target PXR yield is suppressed due to the anomalous properties of X-ray wave responsible for PXR formation. This wave appearing as a consequence of the boundary conditions for the diffracted component of an emitting particle equilibrium electromagnetic field at out-surface of the crystalline target transfers its energy from out-surface where the forward PXR in a vacuum behind the target is formed to the in-surface. As this takes place PXR yield decreases.

Performed calculations have shown the very strong dependence of the forward PXR angular density on the energy of emitting particles. In the region of small energies $\gamma < \gamma_* = \omega_B/\omega_0$ PXR angular density is proportional to $\gamma^6/\gamma_*^6 \ll 1$. On the other hand PXR properties do not depend on γ if $\gamma \gg \gamma_*$ because of the density effect.

The maximum in the forward PXR angular distribution is shifted to the side of small observation angles compared to that for the ordinary PXR emitted to the direction of Bragg scattering. Strong oscillations can be manifested in such a distribution for highly reflecting crystallographic planes.

The problem of the TR background in the task of the forward PXR experimental observation can be solved in part by the suppression of this background in the vicinity of Bragg frequency where the narrow PXR peak is realized due to the negative interference between TR waves emitted from in- and out-surfaces of the target. But in this case the intense narrow TR peak being due to dynamical diffraction effects appears in the range of small observation angles. Such a peak can not be interpreted as PXR peak. One can circumvent this difficulty by using the emission measurements in the range of large enough observation angles where PXR contribution predominates.

It should be noted that an influence of emitting particle multiple scattering is not analyzed in this work because this influence is not essential in the case of thin target under consideration. Moreover, under most appropriate for the experiment condition $\gamma \gg \gamma_*$ the angle of multiple scattering $\Theta_{sc} \sim \gamma^{-1}$ is small compared to the angle corresponding to maximum in PXR angular distribution $\Theta_{max} \sim \gamma_*^{-1}$, therefore the multiple scattering can not change essentially the PXR properties.

Acknowledgements

The authors are thankful to Professor B.M. Bolotovsky for very helpful discussion of the emission of waves with anomalous dispersion from fast charged particles. This work was supported in part by the grants TOO-7.3.-456 from Russian Ministry of Education and UR.02.01.012, UR.02.01.018 from "Universities of Russia" programme.

References

[1] G.M. Garibian, C. Yang, J. Exp. Theor. Phys. 63 (1972) 1198.
[2] V.G. Baryshevsky, I.D. Feranchuk, Phys. Lett. A 57 (1976) 183.
[3] V.G. Baryshevsky, I.D. Feranchuk, J. Phys. (Paris) 44 (1983) 913.
[4] A. Caticha, Phys. Rev. B 45 (1992) 9541.
[5] C.L. Yuan Luke, P.W. Alley, A. Bamberger, G.F. Dell, H. Uto, Nucl. Instr. and Meth. A 234 (1985) 426.
[6] B.N. Kalinin, G.A. Naumenko, D.V. Padalko, A.P. Potylitsin, I.E. Vnukov, Nucl. Instr. and Meth. B 173 (2001) 253.
[7] G. Kube, C. Ay, H. Backe, N. Clawiter, M. Ghazaly, F. Hagenbuck, K.-H. Kaiser, O. Kettig, W. Lauth, H. Manuweiler, D. Schroff, Th. Walcher, T. Weber, Abstracts V Int. Symp. Radiation from Relativistic Electrons in Periodic Structures, 10–24 September 2001, Lake Aya, Altai Mountains, Russia.
[8] V.G. Baryshevsky, Nucl. Instr. and Meth. B 122 (1997) 13.
[9] Z. Pinsker, Dynamical Scattering of X-rays in Crystals, Springer, Berlin, 1984.
[10] A. Cathcha, Phys. Rev. A 40 (1989) 4322.
[11] X. Artru, P. Rullhusen, Nucl. Instr. and Meth. B 145 (1998) 1;
Nucl. Instr. and Meth. B 173 (2001) 16.
[12] N. Imanishi, N. Nasonov, K. Yajima, Nucl. Instr. and Meth. B 173 (2001) 227.
[13] A. Afanas'ev, M. Aginian, J. Exp. Theor. Phys. 74 (1978) 570.
[14] G.M. Garibian, C. Yang, X-ray Transition Radiation, USSR, Erevan, 1983 (in Russian).